Advanced Ferroelectric Modeling for BEOL Negative Capacitance Nanoelectromechanical Switches

Collin Finnan*†
*Department of Electrical Engineering and Computer Sciences
†Kavli Energy and Nanoscience Institute
University of California, Berkeley
Berkeley, CA 94720-1770, USA
collinfinnan@berkeley.edu

Lars Tatum*†
*Department of Electrical Engineering and Computer Sciences
†Kavli Energy and Nanoscience Institute
University of California, Berkeley
Berkeley, CA 94720-1770, USA
lpt@berkeley.edu

Tsu-Jae King Liu*†
*Department of Electrical Engineering and Computer Sciences
†Kavli Energy and Nanoscience Institute
University of California, Berkeley
Berkeley, CA 94720-1770, USA
tsujae@berkeley.edu

2024 International Conference on Simulation of Semiconductor Processes and Devices (SISPAD) | 979-8-3315-1635-2/24/$31.00 ©2024 IEEE | DOI: 10.1109/SISPAD62626.2024.10733007

***Abstract*— Negative capacitance (NC) - achieved by adding a ferroelectric layer in series with the dielectric layer (air gap) of an electrostatic actuator - has been proposed as a means of reducing the pull-in voltage of a nano-electro-mechanical (NEM) switch without physically scaling down the gap size. This paper introduces a two-dimensional device simulation framework for NC NEM switches using the ferroelectric material hafnium zirconium oxide. The ferroelectric layer is simulated using both a simplified single polarization domain model and two different multi-domain models. While a dramatic reduction in pull-in voltage is confirmed for a single-domain ferroelectric, this benefit is predicted to be diminished for a multi-domain ferroelectric.**

Keywords*— *Negative capacitance, nano-electro-mechanical switches, ferroelectric hafnium zirconium oxide, multi-domain ferroelectric modeling

I. Introduction

Back-end-of-line (BEOL) nano-electro-mechanical (NEM) switches have been explored for low-power integrated circuit (IC) applications due to their abrupt switching characteristic, zero off-state leakage current, and ease of monolithic integration [1]. A NEM switch (Fig. 1a) consists of a conductive, moveable beam (source / S) that is electrostatically actuated by applying an input voltage (V_{IN}) to a control electrode (gate / G) to bring it into physical contact with a second conducting electrode (drain / D). Recently, BEOL copper interconnect layers in a foundry complementary metal-oxide-semiconductor (CMOS) IC manufacturing process have been used to form NEM switches with turn-on ("pull-in") voltage (V_{PI}) in the range 3-5 V [2]. Lower voltage operation is desirable for compatibility with CMOS digital logic transistors, however. This can be achieved by scaling down the actuation air-gap size (*i.e.*, the as-fabricated distance between the source and gate electrodes), but this approach presents some practical challenges [3].

The addition of a ferroelectric (FE) capacitor in series with the air-gap dielectric (DE) capacitor of a NEM actuator to leverage the negative capacitance (NC) effect [4] has been proposed as a means for reducing the *effective* air-gap size in NEM systems [5] (Fig. 1b). NC occurs due to a region of negative permittivity in the energy landscape of an FE material. By matching the FE capacitance to the DE capacitance, the overall capacitance of the system is enhanced (Fig. 1c) due to a voltage amplification effect (Fig. 1d). For a limited gate-voltage range of operation, the voltage across the DE is larger than V_{IN}, lowering the value of V_{IN} required to turn on the switch (Fig. 1d).

Hafnium zirconium oxide ($Hf_{0.5}Zr_{0.5}O_2$ / HZO) is a promising FE material for NC applications due to its compatibility with CMOS manufacturing and its scalability to < 10 nm thicknesses. Previous NC NEM switch studies have modeled the FE layer as either having a single polarization domain (SD), using the one-dimensional (1D) steady-state Landau-Khalatnikov (LK) theory [6], or as having numerous parallel 1D domains with statistically varied LK parameters [7]. Recent work has shown, however, that HZO forms nanometer-scale *anti-parallel* domains [8], requiring more sophisticated FE modeling. In this work, a 2D simulation framework for HZO-based NC NEM switches is presented and used to show that the reduction in V_{PI} predicted for the incorporation of a multi-domain (MD) FE layer is dramatically smaller than that predicted for the incorporation of a single-domain (SD) FE layer.

II. Ferroelectric Simulation Methods

A. Negative Capacitance Modeling

Ferroelectric NC behavior is modeled by solving a two-variable system involving the polarization (P) and electric field (E). First, a local P-E model is defined for the domain structure and switching behavior of the FE layer. This local P-E model is then self-consistently solved with Poisson's equation (1) globally throughout the system:

$$\nabla \cdot \left(\epsilon_r \epsilon_0 \boldsymbol{E}(\boldsymbol{r}) + \boldsymbol{P}(\boldsymbol{r})\right) = \boldsymbol{\rho}(\boldsymbol{r}) \quad , \tag{1}$$

where ϵ_r is the relative permittivity and ρ is the surface charge density. In this work, three P-E models are considered: one SD model and two MD models. NC is observed by applying an external voltage to the system to induce FE switching and then evaluating the resultant electrostatic variables. The NC regime is defined as regions of operation wherein P and E within the FE have opposite signs. Note that in each simulation, it is assumed that the FE c-axis is aligned with the system z-axis such that $P_x = P_y = 0$ and $\boldsymbol{P} \rightarrow P = P_z$. Additionally, P is

This work was supported by Samsung Electronics.

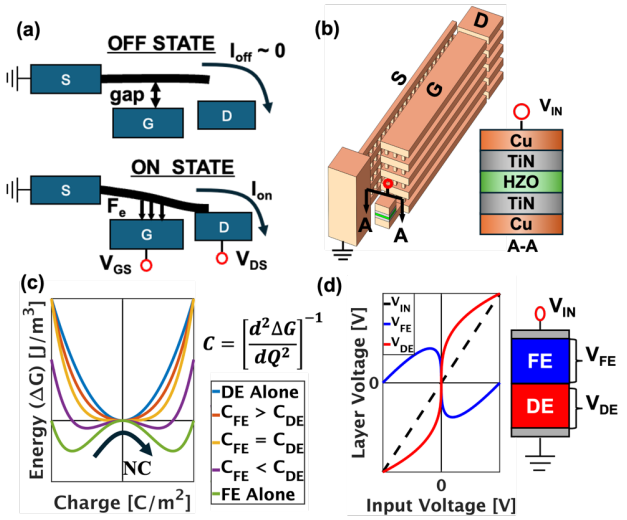

Fig. 1. **NC NEM switch overview.** (a) NEM switch cartoon. (b) Proposed BEOL NC NEM switch made from multiple copper interconnect layers and having a series-connected FE HZO capacitor. (c) Gibb's free energy landscape of FE+DE stack showing the NC effect for various levels of capacitance matching. (d) DE voltage amplification effect due to negative permittivity of the FE layer.

initially spatially randomized in the range $\pm 0.1\ C/cm^2$, and the system naturally evolves into a SD or MD state. Finally, $P = 0$ is assumed outside of the FE layer.

In the simplified steady-state SD NC model (Fig. 2b), P is spatially independent, defined by the 1D-LK equation (2):

$$E_z = \alpha P + \beta P^3 + \gamma P^5 \tag{2}$$

where $\alpha, \beta,$ and γ are Landau fitting parameters and E_z is the z-component of $\boldsymbol{E}$. Because α is negative, there is NC for small P, and the P-E curve takes the shape of a single "S" (Fig. 2e). When there is no externally applied electric field, $P = 0$ within the FE layer, as this is the lowest energy state for a well-matched FE+DE stack (see Fig. 1c).

In MD HZO systems, two NC modalities exist: *extrinsic NC* (Fig. 2c) due to domain wall motion [9] and *intrinsic NC* (Fig. 2d) due to domain nucleation [10]. Extrinsic NC is modeled by solving the time-dependent Ginzburg-Landau (TDGL) equation (3):

$$-\Gamma \frac{\partial P(\boldsymbol{r})}{\partial t} =$$

$$\alpha P(\boldsymbol{r}) + \beta P(\boldsymbol{r})^3 + \gamma P(\boldsymbol{r})^5 - k\nabla^2 P(\boldsymbol{r}) - E_z(\boldsymbol{r}) \tag{3}$$

where Γ is the kinetic coefficient and k is a gradient coefficient describing the energy between adjacent domains. For sufficiently small k values, domain wall energies become negligible, and antiparallel domains form such that the *net* polarization in the FE layer is 0. In contrast, intrinsic NC assumes discrete, *immobile* domains, which can be modeled using a modified TDGL equation, wherein $P(r) \rightarrow P_i(r)$ is the polarization in the predefined i^{th} domain and k is set arbitrarily large to prevent extraneous domains. Extrinsic NC models

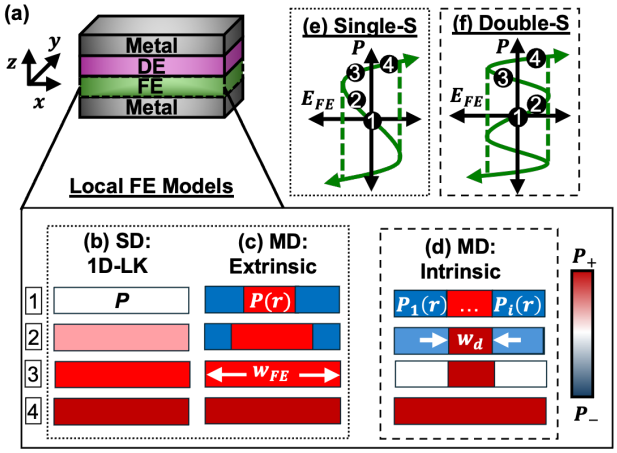

Fig. 2. **NC models.** (a) FE+DE capacitor. (b) SD P switching. (c) MD extrinsic P switching. (d) MD intrinsic P switching. (e) P-E for SD and extrinsic MD models. (f) P-E for intrinsic MD model.

result in a single-S P-E curve, while intrinsic NC models exhibit a double-S P-E curve due to the initial linear dielectric response of parallel domains (Fig. 2f). Experimental results measuring the P-E curve of HZO have shown both double [10] and single [11] S-curves; thus, both NC polarization switching modalities are investigated herein.

B. Effect of Metal Interlayer

Capacitance matching for NC NEM switches is practically achieved by setting the area of the FE capacitor to be smaller than that of the air-gap capacitor, necessitating a metal interlayer (MI) to redistribute charge. Fundamentally, the MI delocalizes $E_{FE}(\boldsymbol{r})$, introducing a plane of equipotential across the entire FE layer. Reports of experimentally observed NC in FE+DE capacitor stacks with a MI have been both confirmed [12] and denied [13]; therefore, it is worthwhile to investigate the effect of the MI on NC, using the various NC models.

Simulations were run using the COMSOL® Multiphysics finite element method (FEM) tool with a square mesh of 0.25 nm. Both metal-ferroelectric-dielectric insulator-metal (MFIM) and MF**MI**M capacitors comprised of HZO and aluminum oxide (Al_2O_3 / AO) FE+DE stacks were simulated using SD, MD extrinsic NC, and MD intrinsic NC models (Fig. 3a). HZO parameter values taken from [9] are listed in Table I. MD simulations were run once with uniform Landau parameters and again with parameters randomized by 1% across domains to account for coercive field (E_C) variability and non-uniform domain nucleation. The simulated 2D capacitors were 100 nm in width, and intrinsic NC simulations assumed a domain width of 10 nm. P and E were evaluated by averaging their value throughout the entire FE layer.

NC in the MFIM and MFMIM capacitor stacks (Fig. 3a) was evaluated by applying 1 kHz voltage pulses across the device terminals and observing the resultant P-E curve. It should be noted that when the saturation value of polarization (P_S) is reached, the FE becomes single domain and does not return to a MD state until the applied voltage is removed; therefore, the P-E return trace for MD simulations is identical

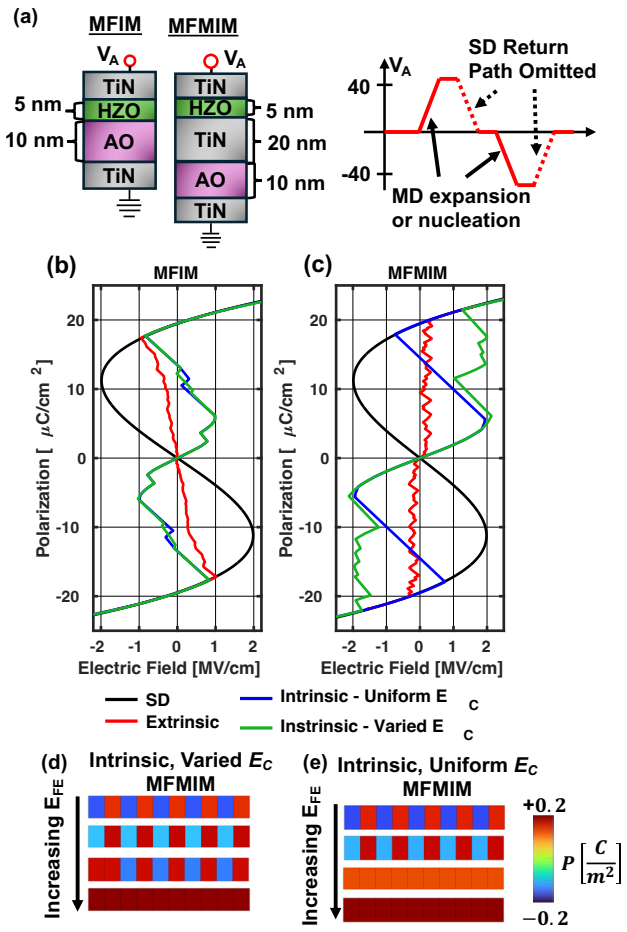

Fig. 3. **NC metal interlayer effect.** (a) MFIM and MFMIM capacitor simulation setup showing the applied voltage (V_A) waveform. The P-E return traces from $P = \pm P_S$ to $P = 0$ are omitted for clarity. (b) MFIM P-E curves showing the expected NC behavior for each model. E_C variability has little effect on NC. (c) MFMIM P-E curves, showing that the metal interlayer negates NC for non-uniform switching modalities. (d) Domain structure during MD intrinsic switching with varied E_C, illustrating the charge redistribution and repolarization phenomenon. (e) Domain structure during MD intrinsic switching with uniform E_C.

to that for SD simulation and is omitted in Figs. 3(b) and 3(c) for clarity.

MFIM simulations (Fig. 3b) result in expected P - E relationships, but MFMIM simulations (Fig. 3c) exhibit MD amplification only for a uniform-E_C intrinsic NC model. The extrinsic and varied-E_C intrinsic NC models show small regions of negative permittivity associated with individual domains expanding or switching, respectively; however, because charge redistributes on the metal interlayer, the magnitude of E across the entire FE layer decreases after each domain switches, repolarizing the remaining antiparallel domains (Fig. 3d). In contrast, switching is synchronized for uniform-E_C intrinsic NC simulations (Fig. 3e), allowing net voltage amplification across the DE layer.

III. NC NEM Switch Design and Simulation

2D BEOL NEM switch pull-in simulations (Fig. 4) were performed with a MFM capacitor connected in series with the air-gap capacitor, using SD *vs*. MD uniform-E_C intrinsic NC models. (Out-of-plane dimensions were not accounted for, and extrinsic and varied-E_C MD NC models were omitted since they do not provide for voltage amplification in the MFMIM configuration.) The NEM switch was designed for a 16 nm process technology with minimum half-pitch $F = 32\,nm$ (Table II). A static boundary condition was applied to the cantilever anchor. Poisson's equation was solved globally while the P-E relationship and Maxwell's stress tensor were solved for the FE and NEM switch, respectively. The applied voltage (V_{IN}) was a slow ramp function such that at each point in time the quasi-static beam displacement, polarization, and electric field were self-consistently calculated. Beam displacement was found by coupling the stress tensor with the mechanical material properties of copper (Young's modulus, E_{cu}, Poisson's ratio, ν_{Cu}, and volumetric density, ρ_{Cu}) using the COMSOL® Electromechanics toolbox.

TABLE I. Simulation Parameters

HZO Parameters			NEM Switch Parameters		
Term	Value	Unit	Term	Value	Unit
α	-2.5×10^{9}	m/F	F	32	nm
β	6×10^{10}	$m^5/(F\cdot C^2)$	t_M	70	nm
γ	1.5×10^{11}	$m^9/(F\cdot C^4)$	t_{via}	50	nm
Γ	100	$1/(\Omega\cdot m)$	l_{beam}	$60F$	nm
g	1×10^{-10}	m^3/F	t_{beam}	$2.2F$	nm
ϵ_{HZO}	$24\epsilon_0$	F/m	l_{act}	$52F$	nm
$\epsilon_{Al_2O_3}$	$10\epsilon_0$	F/m	t_{gap}	$2.5F$	nm
w_{FE}	100	nm	t_{cont}	$1.1F$	nm
w_d	10	nm	E_{Cu}	120	GPa
N	10	–	ν_{Cu}	0.34	–
t_{AO}	10	nm	ρ_{Cu}	8960	kG/m^3
t_{HZO}	5	nm			

IV. Pull-In Voltage Analysis Results

A. Single Domain

Fig. 5a shows that, for the SD model, V_{PI} decreases with increasing FE thickness (t_{FE}); specifically, with the incorporation of a FE capacitor, V_{PI} can be reduced from 2.5 V to less than 0.8 V at t_{FE} =11 nm. Fig. 5b shows that this is the upper limit for the FE+DE stack to maintain stable NC behavior. For $t_{FE} = 12$ nm and $t_{FE} = 13$ nm, the beam displacement is non-zero for $V_{IN} = 0$ due to spontaneous polarization within the HZO. Energetically, the system has a double-well energy-*vs*.-charge characteristic (cf. Fig. 1c, $C_{FE} < C_{DE}$), meaning even with no applied voltage, there is differential

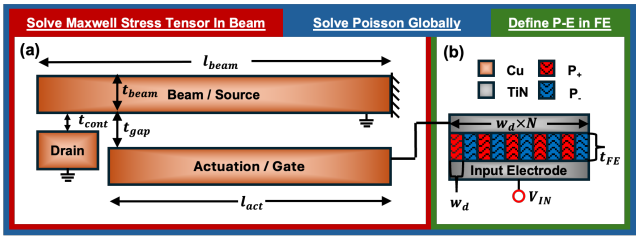

Fig. 4. **NC NEM switch simulation framework.** (a) 2D plan-view of BEOL NEM switch, solved using Maxwell stress tensor. (b) HZO capacitor electrically connected to NEM switch gate electrode, solved using 1D-LK or modified TDGL.

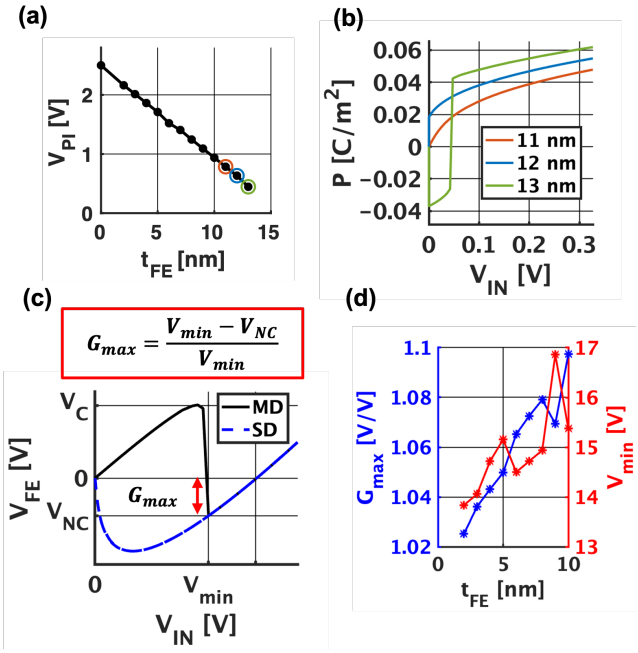

Fig. 5. **NC NEM switch pull-in analysis.** (a) SD V_{PI} v. t_{FE} (b) P v. V_{IN} for various t_{Fe} showing spontaneous polarization due to poor capacitance matching. (c) Comparison of NC voltage amplification effect in a SD v. MD intrinsic model. (d) MD G_{max} and V_{min} v. t_{FE} highlighting minimal NC benefits using an MD model.

charge across the actuation electrodes. Thus, although a thicker FE layer could further lower V_{PI}, there is a practical limit due to stability considerations.

B. *Multi-Domain Intrinsic NC Model*

Fig. 5c compares how the voltage across the FE layer depends on V_{IN} using MD intrinsic *vs.* a SD NC model. Because there is a region of positive permittivity in the double-S P-E characteristic of the MD intrinsic model, the NC effect does not appear until V_{IN} exceeds a minimum voltage V_{min}. Moreover, the maximum possible voltage gain across the air-gap (G_{max}) is attenuated for the MD intrinsic *vs*. the SD NC models. Fig. 5d shows how G_{max} and V_{min} each increase with t_{FE}, indicating a tradeoff for achieving lower V_{PI}. For the NC NEM switch design in this work, V_{min} is 5-7× larger than V_{PI} for the NEM switch alone, meaning that during pull-in, the applied voltage is primarily dropped across the FE rather than the air-gap. Even if NC were to be achieved within a reasonable gate voltage range, G_{max} would only be 2-10%, leading to smaller improvements in V_{PI} relative to the ~3× reduction in V_{PI} observed for the SD FE.

V. Conclusion

A 2D simulation framework for negative capacitance (NC)-assisted NEM switches is developed and used to elucidate fundamental challenges for their practical implementation. Simulations using an idealized ferroelectric (FE) layer having a single domain predict substantial voltage amplification across the NEM actuation air-gap, reducing the pull-in voltage V_{PI} by 3×. In contrast, more realistic multi-domain FE simulations using extrinsic and intrinsic NC models reveal that NC may not be achievable due the need for a metal interlayer (MI) to achieve capacitance matching, unless FE switching is synchronized across the multi-domains. Moreover, the reduction in V_{PI} using a synchronized MD FE layer is projected to be < 10%, or 30 × smaller than that predicted for a SD FE layer. Further work is required to better understand NC-NEM systems, including 3D simulations for realistic capacitance matching and experimental work to characterize the impacts of the metal interlayer on NC.

Acknowledgment

The authors thank Urmita Sikder for valuable discussions regarding BEOL NEM switches and the Salahuddin group at UC Berkeley for helpful conversations regarding NC. The authors also thank the Kavli Energy and Nanoscience Institute (ENSI) for providing computation resources.

References

[1] U. Sikder and T. -J. King Liu, "3D Integrated CMOS-NEM Systems: Enabling Next-Generation Computing Technology," in 2021 IEEE International Meeting for Future Electron Devices, Kansai (IMFEDK), Nov. 2021, pp. 1–4. doi: 10.1109/IMFEDK53601.2021.9637634.

[2] U. Sikder, R. Naous, V. Stojanović, and T. -J. K. Liu, "Non-Volatile Nano-Electro-Mechanical Switches and Hybrid Circuits in a 16 nm CMOS Back-End-of-Line Process," IEEE Electron Device Letters, vol. 44, no. 1, pp. 136–139, Jan. 2023, doi: 10.1109/LED.2022.3221701.

[3] U. Sikder, G. Usai, T.-T. Yen, K. Horace-Herron, L. Hutin, and T.-J. K. Liu, "Back-End-of-Line Nano-Electro-Mechanical Switches for Reconfigurable Interconnects," IEEE Electron Device Lett., vol. 41, no. 4, pp. 625–628, Apr. 2020, doi: 10.1109/LED.2020.2974473.

[4] S. Salahuddin and S. Datta, "Use of Negative Capacitance to Provide Voltage Amplification for Low Power Nanoscale Devices," Nano Lett., vol. 8, no. 2, pp. 405–410, Feb. 2008, doi: 10.1021/nl071804g.

[5] M. Masuduzzaman and M. A. Alam, "Effective Nanometer Airgap of NEMS Devices Using Negative Capacitance of Ferroelectric Materials," Nano Lett., vol. 14, no. 6, pp. 3160–3165, Jun. 2014, doi: 10.1021/nl5004416.

[6] C. Yoon, J. Min, J. Shin, and C. Shin, "Device Design Guideline for HfO_2-Based Ferroelectric-Gated Nanoelectromechanical System," IEEE J. Electron Devices Soc., vol. 8, pp. 608–613, 2020, doi: 10.1109/JEDS.2020.3001272.

[7] C. Yoon and C. Shin, "Electrical Characteristics of Nanoelectromechanical Relay with Multi-Domain HfO2-Based Ferroelectric Materials," Electronics, vol. 9, no. 8, p. 1208, Jul. 2020, doi: 10.3390/electronics9081208.

[8] T. K. Paul, A. K. Saha, and S. K. Gupta, "Head-to-Head and Tail-to-Tail Domain Wall in Hafnium Zirconium Oxide: A First Principles Analysis of Domain Wall Formation and Energetics," 2023, doi: 10.48550/ARXIV.2305.12350.

[9] P. Kumar, A. Nonaka, R. Jambunathan, G. Pahwa, S. Salahuddin, and Z. Yao, "FerroX: A GPU-accelerated, 3D phase-field simulation framework for modeling ferroelectric devices," Computer Physics Communications, vol. 290, p. 108757, Sep. 2023, doi: 10.1016/j.cpc.2023.108757.

[10] M. Hoffmann et al., "Intrinsic Nature of Negative Capacitance in Multidomain Hf 0.5 Zr 0.5 O 2 - Based Ferroelectric/Dielectric Heterostructures," Adv Funct Materials, vol. 32, no. 2, p. 2108494, Jan. 2022, doi: 10.1002/adfm.202108494.

[11] M. Hoffmann et al., "Unveiling the double-well energy landscape in a ferroelectric layer," Nature, vol. 565, no. 7740, pp. 464–467, Jan. 2019, doi: 10.1038/s41586-018-0854-z.

[12] Y.-S. Jiang et al., "Operation bandwidth of negative capacitance characterized by the frequency response of capacitance magnification in ferroelectric/dielectric stacks," J. Mater. Chem. C, vol. 9, no. 4, pp. 1401–1409, 2021, doi: 10.1039/D0TC04025H.

[13] H. W. Park et al., "Exploring the Physical Origin of the Negative Capacitance Effect in a Metal–Ferroelectric–Metal–Dielectric Structure," Adv Funct Materials, vol. 33, no. 51, p. 2304754, Dec. 2023, doi: 10.1002/adfm.202304754.